Transverse tubular network structures in the genesis of intracellular calcium alternans and triggered activity in cardiac cells

Zhen Song, Michael B. Liu, Zhilin Qu

Supplemental Information

1. Three-dimensional cell model

The cell model is a three-dimensional (3D) grid of Ca^{2+} release units (CRUs) with CRU spacing being 1.84 μm in the longitudinal direction and 0.9 μm in the transverse direction (Fig.S1). The control cell size is $L_x \times L_y \times L_z = 64 \times 32 \times 16 = 32{,}768$ CRUs, corresponding to a dimension of $118 \times 29 \times 14$ μm^3. We varied L_z to investigate the effects of cell size. Intracellular sodium concentration ($[Na^+]_i$) was fixed to 12 mM. The details of this model can be found in our previous studies [1, 2]. The equations and parameters are the same as in our previous study [2] except for the changes described in detail below.

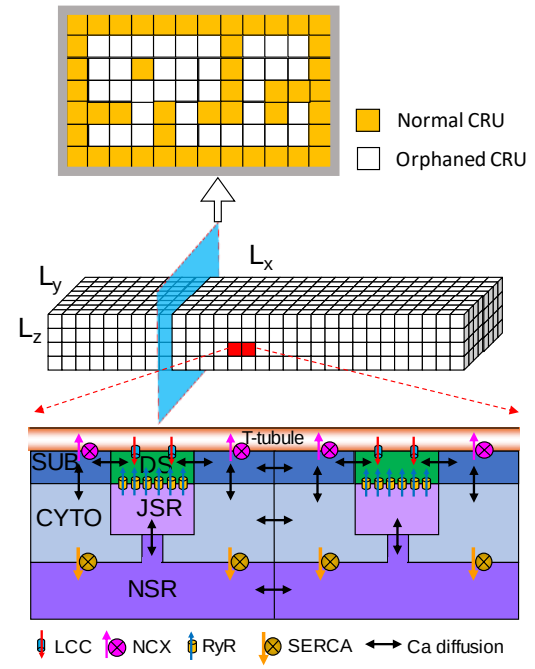

Fig.S1. Schematic of the 3D cell model. Top: a 2D slice through the 3D cell, where yellow and white represent normal and orphaned CRUs. Middle: a single cell consists of $L_x \times L_y \times L_z$ CRUs arranged in a 3D grid. Bottom: the coupling between different compartments and CRUs. DS—dyadic space, SUB—sub-membrane space, CYTO—cytosolic space, NSR—network SR, and JSR—junctional SR.

Voltage and ionic currents

For simplicity, we assume that all the ionic channels are equally distributed on the transvers tubular (TT) network and sarcolemmal membranes. Therefore, the differential equation for membrane potential (V) is

$$C_m \frac{dV}{dt} = -\frac{1}{N(1-\phi_{total})}\sum_{k=1}^{N(1-\phi_{total})}\left(i_{Na} + i_{K1} + i_{Kr} + i_{Ks} + i_{to,f} + i_{to,s} + i_{NaK} + i_{Ca,L} + i_{NCX}\right) - I_{sti}, \quad \text{(S1)}$$

where C_m=1 μF/cm^2 is the membrane capacitance; N is the total number of CRUs, i.e., N= $L_x \times L_y \times L_z$; ϕ_{total} is the ratio of orphaned CRUs (OCRUs) in a cell as the number of OCRUs against the total CRUs, which is defined in Eq.1 in the main text; the lower case *i's* in Eq.S1 are the current densities of the ion channels in each CRU; and I_{sti}=-50 μA/cm^2 is the stimulus current density. Since the densities of the Ca^{2+}-independent currents are identical in each CRU, Eq.S1 becomes,

$$C_m \frac{dV}{dt} = -\frac{1}{N(1-\phi_{total})}\sum_{k=1}^{N(1-\phi_{total})}\left(i_{Ca,L} + i_{NCX}\right) - \left(I_{Na} + I_{K1} + I_{Kr} + I_{Ks} + I_{to,f} + I_{to,s} + I_{NaK}\right) - I_{sti}. \quad \text{(S2)}$$

where the upper case *I*'s are the whole-cell current densities. For simplicity, we assumed that I_{Ks} depends on the whole-cell averaged Ca^{2+} concentration not the local concentrations. Therefore, under our assumption that the ion channels are uniformly distributed, different TT network structures have no effect on the current densities of the Ca^{2+}-independent ionic currents. Although, both LCC and NCX do depend on local Ca^{2+} and thus on the TT network structure, the effects on the whole-cell current densities are small, as shown in Fig.S2.

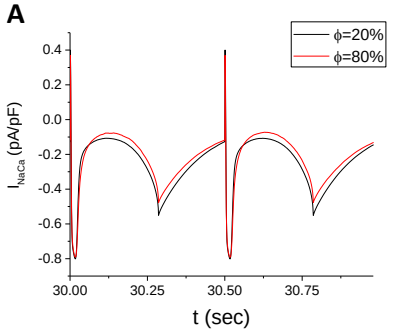

Fig.S2. Effects of TT network structure on whole-cell current densities for 20% OCRUs (black) and 80% OCRUs (red). **A**. NCX. **B**. LCC.

Local Ca^{2+} dynamics

The equations for local Ca^{2+} dynamics are listed below, which are the same as in our previous model [2] except that the OCRUs lack both LCCs and NCX:

$$\frac{dc_i}{dt} = \beta_i(c_i)\left(j_{dsi}\frac{v_s}{v_i} - j_{up} + j_{leak} - j_{TCi} + j_{ci}\right),$$
$$\frac{dc_s}{dt} = \beta_s(c_s)\left(j_{dps}\frac{v_p}{v_s} + \xi j_{NCX} - j_{dsi} - j_{TCs} + j_{cs}\right),$$
$$\frac{dc_p}{dt} = \beta_p(c_p)\left(j_{rel} + \xi j_{Ca,L} - j_{dps}\right),$$
$$\frac{dc_{nsr}}{dt} = \left(j_{up} - j_{leak}\right)\frac{v_i}{v_{nsr}} - j_{tr}\frac{v_{jsr}}{v_{nsr}} + j_{cnsr},$$
$$\frac{dc_{jsr}}{dt} = \beta_{jsr}(c_{jsr})\left(j_{tr} - j_r\frac{v_p}{v_{jsr}}\right),$$

where

$$\xi = \begin{cases} 0, & orphaned\ CRU \\ 1, & otherwise \end{cases}$$

The j's in the equations above are Ca^{2+} fluxes.

2. Modeling TT network structures

Uniformly and non-uniformly random TT network structures were generated using three different numerical algorithms described in detail below.

Uniformly random TT networks

To generate uniformly random TT network structures, we assigned LCC-NCX clusters randomly to the CRUs using a uniform distribution excluding the outermost layer. The OCRU ratio was determined by the probability of LCC-NCX placement.

Non-uniform TT networks

We used a 3D random walk algorithm to construct the non-uniform TT network structures. Each walk first started from a random CRU location on the sarcolemmal surface. Next, for each step, the walk randomly moved to one of the six nearest neighboring CRUs, with four in the transverse and two in the longitudinal directions. This algorithm is controlled by the following 3 parameters: 1) The number of steps of each random walk, denoted as l_s, is set to a constant value; 2) The total number of random walks is determined by the OCRU ratio

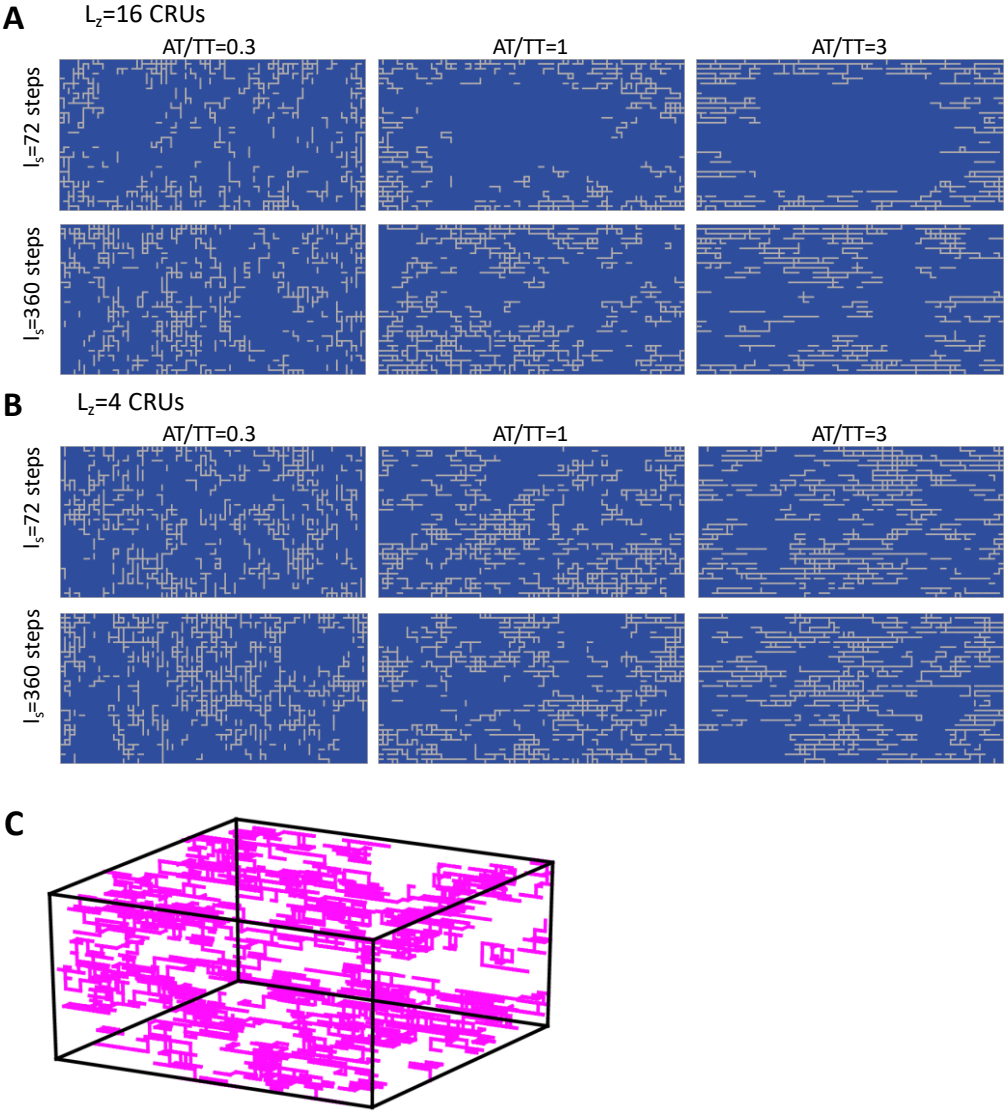

Fig.S3. **Examples of non-uniform TT network structures**. **A.** 2D views of TT networks with ϕ=50%. l_s=72 for the top row and 360 for the bottom. From left to right, AT/TT is 0.3, 1 and 3, respectively. There are 16 CRUs along the z-direction (L_z=16) and the 7th slice is shown for each case. **B.** Same as in A, but L_z=4 and the 2nd slice along the Z-direction. **C**. A 3D view of the TT network generated in a cell with l_s=72, AT/TT=4, ϕ=90%, and L_z=16 CRUs.

denoted as ϕ; 3) Different AT/TT ratios are controlled by assigning different probabilities of walking along the transverse and longitudinal directions (e.g. AT/TT~3, measured in the experiment by Song et al[4]). Fig.S3 A and B show examples of TT network structures generated using this algorithm for different combinations of random walk steps (l_s), and AT/TT ratios with ϕ=50%. Cell thickness (L_z) can also impact the TT network structures this algorithm can generate (hollow structures seen with L_z=16, but not with L_z=4). A 3D view of the TT network in a cell is shown in Fig.S3C, which is a hollow structure. However, since the ATs and TTs are distributed close to the cell surface, it is hard to see the hollow structure in the 3D view.

Sheet-like TT networks

The method used to generate T-sheets is illustrated in Fig.S4. First, we randomly choose a CRU (V_1) in an XZ plane where Y=1 or Y=L_y (both on sarcolemmal surfaces) with coordinate (x_1,y_1,z_1). Next, we randomly choose another CRU (V_2) along the Y direction such that the line segment (l) passing through both V_1 and V_2 is perpendicular to the XZ plane. The y-coordinate of V_2 is sampled from a discrete uniform distribution bounded between 1 and L_y. Thus the length of each T-sheet is $\Delta y=y_2-y_1$. For each CRU on l, we randomly generate a line segment along the X direction with its length drawn from a binomial distribution. Together, these line segments combine to form a T-sheet. The parameters of the binomial distribution are chosen such that the average width of a T-sheet is 5 CRUs (~10 μm), which matches the recent experimental observation[5]. By changing the total number of generated T-sheets, we can vary the OCRU ratio of the TT network.

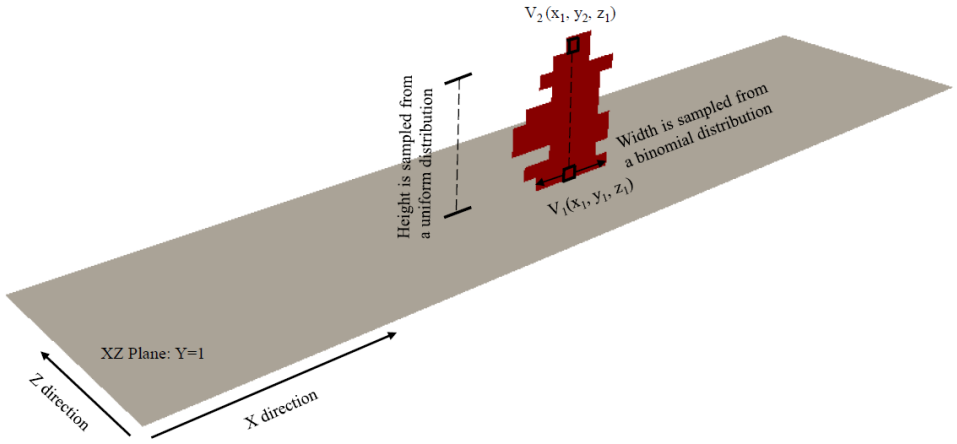

Fig.S4. Illustration of the algorithm for generating a T-sheet.

3. Pacing protocol and parameters for alternans

To simulate Ca^{2+} alternans, we paced the cell for 60 beats at a PCL of 360 ms under AP clamp. The clamped AP waveform (Fig.S5) is described by the following time-dependent function taken from Chudin et al [6]:

$$V(t)=\begin{cases} V_{min}+(V_{max}-V_{min})\sqrt{1-(\frac{t-mT}{xT})^2}\ , & mT \le t \le mT+xT \\ V_{min}, & mT+xT < t \le (m+1)T \end{cases},$$

where V_{min} =-80 mV is the resting potential and V_{max}=10 mV *is* the peak voltage.

The parameters that were changed from our previous study [2] to generate Ca^{2+} alternans are listed in Table S1.

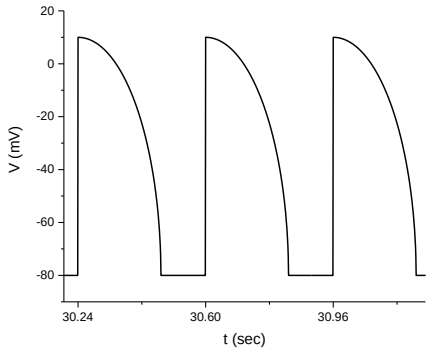

Fig.S5. Time trace of a clamped AP waveform at a pacing cycle length of 360 ms.

Table S1. Altered parameters to induce Ca^{2+} alternans

Parameter	Definition	Unit	Value
v_{up}	Strength of uptake	$\mu M\ ms^{-1}$	0.36
N_{LCC}	Number of LCCs		6
v_{NaCa}	Strength of exchanger current	$\mu M\ ms^{-1}$	7
K_u	Calsequestrin-unbound opening rate of RyRs	$\mu M^{-2}\ ms^{-1}$	3.8×10^{-4}
K_b	Calsequestrin-bound opening rate of RyRs	$\mu M^{-2}\ ms^{-1}$	5×10^{-5}

4. Pacing protocol and parameters for triggered activity

To simulate Ca^{2+}-mediated triggered activity, we paced the cell for 40 beats to reach steady state at a PCL of 300 ms under free running AP. The parameters that were changed from our previous study [2] to generate Ca^{2+} waves and triggered activity are listed in Table S2.

Table S2. Altered parameters to induce Ca^{2+} waves and TA

Parameter	Definition	Unit	Value
v_{up}	Strength of uptake	$\mu M\ ms^{-1}$	0.72
N_{LCC}	Number of LCCs		10
v_{NaCa}	Strength of exchanger current	$\mu M\ ms^{-1}$	21
K_u	Calsequestrin-unbound opening rate of RyRs	$\mu M^{-2}\ ms^{-1}$	1.33×10^{-3}
K_b	Calsequestrin-bound opening rate of RyRs	$\mu M^{-2}\ ms^{-1}$	1.75×10^{-4}

5. Numerical methods

The differential equations were numerically solved using an Euler method with a fixed time step of 0.01 ms. The gating variables were integrated using the method by Rush and Larsen [7]. The LCCs and RyRs were simulated using a variant of Gillespie's method developed by Nivala et al [8]. All computer programs were coded in CUDA, and simulations were carried out on Nvidia Tesla K20 and K80 Graphics Processing Units (GPUs).

6. Effects of TT density on Ca^{2+} transient and SR Ca^{2+} load

We used the uniformly random TT network structures (e.g., Fig.1E) to investigate the effects of TT density on Ca^{2+} transient and SR Ca^{2+} load. Fig.S6A shows line scans of local cytosolic Ca^{2+} concentration and whole-cell averaged Ca^{2+} concentration ($[Ca^{2+}]_i$) with the control RyR open probability for three different ϕ values respectively. When all the CRUs were coupled with their associated LCC-NCX clusters (ϕ=0, no OCRUs), Ca^{2+} release was synchronous and the peak $[Ca^{2+}]_i$ was ~3 μM. When ϕ=50%, the Ca^{2+} release became dyssynchronous and the peak $[Ca^{2+}]_i$ reduced to ~2.5 μM. If ϕ=100% (all CRUs were OCRUs except in the outermost layer), Ca^{2+} release only

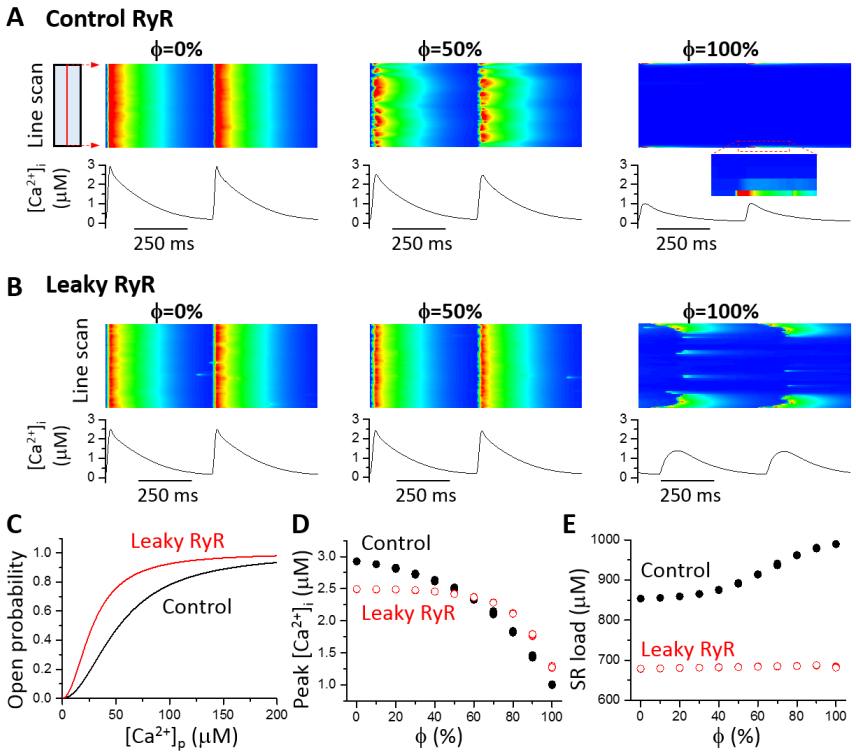

Fig.S6. Effect of OCRU ratio on Ca^{2+} cycling properties. **A**. Line scan and $[Ca^{2+}]_i$ versus time for ϕ=0, 50%, and 100% with control RyR open probability (black curve in C). PCL=500 ms. **B**. Same as A but with an increased leaky RyR open probability (red curve in C). **C**. RyR open probability versus the Ca^{2+} concentration in the dyadic space ($[Ca^{2+}]_p$) for both control and leaky RyRs. Parameters for control RyRs are the same as in our previous study [3], and leaky RyRs were modeled by increasing the closed-to-open rate three-fold. **D**. Peak $[Ca]_i$ versus ϕ for control (black) and leaky (red) RyRs. **E**. SR Ca^{2+} load versus ϕ for control (black) and leaky (red) RyRs.

occurred at the boundary layer, and the peak $[Ca^{2+}]_i$ reduced to ~1 μM. Figs. S6 D and E plot the peak $[Ca^{2+}]_i$ and SR Ca^{2+} load versus ϕ respectively, showing that as the ratio of OCRUs was increased, peak $[Ca^{2+}]_i$ decreased while SR load increased.

We then enhanced the RyR open probability by increasing the RyR sensitivity to the Ca^{2+} concentration in the dyadic space (Fig.S6C). When ϕ=0 (no OCRUs), increasing the RyR open probability decreased the peak $[Ca^{2+}]_i$ from ~3 μM to ~2.5 μM (left panel in Fig.S6B), and the SR load decreased from ~850 μM to ~680 μM (Fig.S6E). When ϕ=50%, the peak $[Ca^{2+}]_i$ and SR Ca^{2+} load remained almost unchanged, and the Ca^{2+} release remained synchronous (middle panel in Fig.S6B). The peak $[Ca^{2+}]_i$ started to decrease after ϕ was increased to 60% (Fig.S6D), while the SR load remained at the same level (Fig.S6E). When ϕ=100%, Ca^{2+} waves occurred, propagating from the borders toward the center (right panel in Fig.S6B). Our finding that increasing RyR open probability causes more synchronous Ca^{2+} release agrees with the experimental observation that β-adrenergic stimulation can restore the Ca^{2+} transient of VMs lacking TTs [9].

7. Ca^{2+} alternans with free running APs

We simulated the uniformly random TT network structures with free running APs at different TT densities for L_z=16. For a given TT density, the cell was paced for 90 beats at a PCL of 360 ms. The Ca^{2+} transient peaks of the last 10 beats were plotted against the OCRU ratio ϕ as shown in Fig.S7A. As a comparison, the same plot under the AP clamp condition is also shown in the same figure. It appears that the biphasic relationship between Ca^{2+} alternans and TT density preserves, indicating that our theory explaining the effect of TT disruption on Ca^{2+} alternans remain valid without clamping APs. Furthermore, time traces of AP, Ca^{2+} transient, $I_{Ca,L}$, and I_{NCX} for two consecutive beats in the steady state are shown in Fig.S7B. As seen in the plot, although APD_{90} does not exhibit alternans, AP morphology still exhibits alternating behaviors due to the combined response of $I_{Ca,L}$ and I_{NCX} on Ca^{2+} alternans. With a larger Ca^{2+} transient, $I_{Ca,L}$ appears smaller due to Ca^{2+} dependent inactivation, which results in lower AP plateau (black in Fig.S7B), but I_{NCX} is larger because it extrudes more Ca^{2+} out of the cell, which eventually depolarizes AP to the extent that the APD_{90} is about the same as with a smaller Ca^{2+} transient.

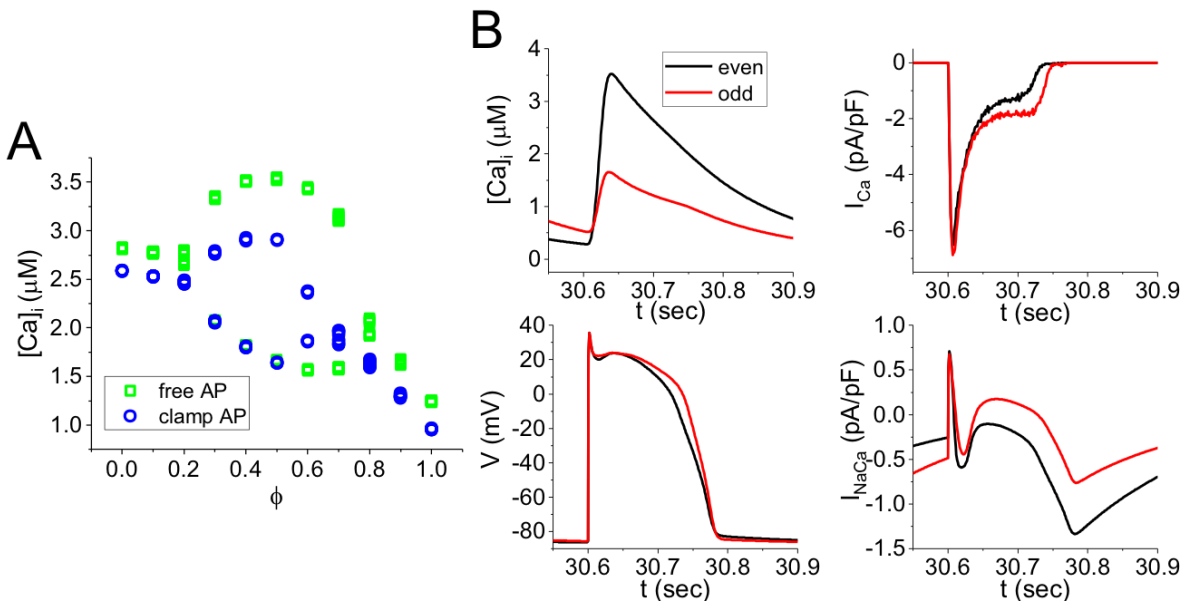

Fig.S7. Ca^{2+} alternans with free running APs. **A**. Ca^{2+} transient peaks for both AP clamp (black circle) and AP free running (red square) conditions vs. the OCRU ratio ϕ. PCL=360 ms. **B**. Time traces of Ca^{2+} transient, AP, I_{Ca}, and I_{NaCa} for two consecutive beats in the steady state with free running APs. ϕ=0.5, and L_z=16.

8. LCC-NCX cluster location and Ca^{2+} alternans

The effect of LCC-NCX cluster location on Ca^{2+} alternans is simulated in two scenarios: i) LCC-NCX clusters are uniformly distributed only on cell membrane (Fig.S8A, left); ii) LCC-NCX clusters are uniformly distributed throughout the cell (Fig.S8B, left). We simulated the two cases under the same conditions. Time courses of Ca^{2+} transient for the two cases are shown in Fig.S8. It appears that distributing LCC-NCX clusters inside the cell promotes Ca^{2+} alternans.

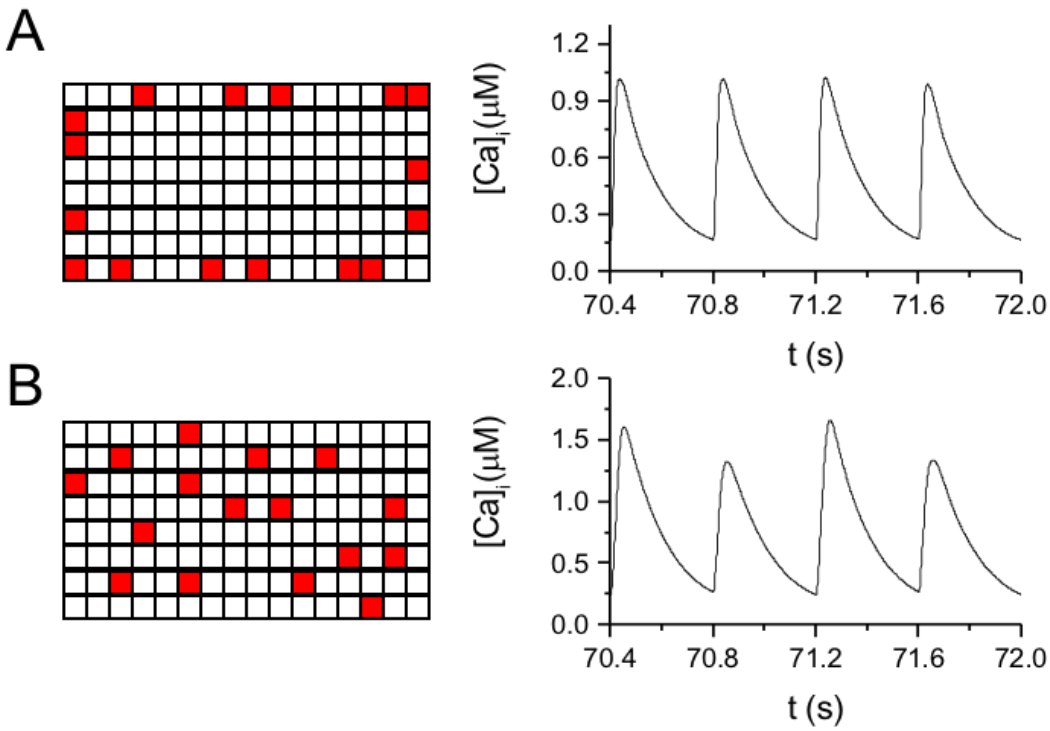

Fig.S8. **LCC-NCX cluster location and Ca^{2+} alternans. A**. LCC-NCX clusters are distributed on cell membrane, and the cell exhibits no Ca^{2+} alternans. **B**. LCC-NCX cluster are uniformly distributed throughout the cell, and the cell exhibits Ca^{2+} alternans. PCL=400 ms, L_x=64, L_y=32, L_z=8, and the number of LCC-NCX clusters assigned is 3277.

References:

[1] Restrepo JG, Weiss JN, Karma A. Calsequestrin-mediated mechanism for cellular calcium transient alternans. Biophysical Journal2008. p. 3767-89.
[2] Song Z, Ko CY, Nivala M, Weiss JN, Qu Z. Calcium-Voltage Coupling in the Genesis of Early and Delayed Afterdepolarizations in Cardiac Myocytes. Biophysical Journal2015. p. 1908-21.
[3] Song Z, Qu Z, Karma A. Stochastic initiation and termination of calcium-mediated triggered activity in cardiac myocytes. Proceedings of the National Academy of Sciences. 2017;114:E270-E9.
[4] Song LS, Sobie EA, McCulle S, Lederer WJ, Balke CW, Cheng HP. Orphaned ryanodine receptors in the failing heart. PNAS: National Acad Sciences; 2006. p. 4305-10.
[5] Seidel T, Navankasattusas S, Ahmad AA, Diakos NA, Xu WD, Tristani-Firouzi M, et al. Sheet-Like Remodeling of the Transverse Tubular System in Human Heart Failure Impairs Excitation-Contraction Coupling and Functional Recovery by Mechanical Unloading. Circulation. 2017.
[6] Chudin E, Goldhaber J, Garfinkel A, Weiss J, Kogan B. Intracellular Ca(2+) dynamics and the stability of ventricular tachycardia. Biophys J. 1999;77:2930-41.
[7] Rush S, Larsen H. A practical algorithm for solving dynamic membrane equations. IEEE Trans Biomed Eng. 1978;25:389-92.
[8] Nivala M, de Lange E, Rovetti R, Qu Z. Computational modeling and numerical methods for spatiotemporal calcium cycling in ventricular myocytes. Front Physiol: Frontiers; 2012. p. 114.
[9] Brette F, Rodriguez P, Komukai K, Colyer J, Orchard CH. beta-adrenergic stimulation restores the Ca transient of ventricular myocytes lacking t-tubules. J Mol Cell Cardiol. 2004;36:265-75.